An Autonomous Microdigital Sun Sensor by a CMOS Imager in Space Application

Ning Xie, *Member, IEEE*, and Albert J. P. Theuwissen, *Fellow, IEEE*

***Abstract*—Digital sun sensors are a category of attitude sensors applied on spacecraft. The proposed microdigital sun sensor (μDSS) is specifically applied for microsatellites. This application requires low power consumption, high accuracy, and radiation hardness, as well as miniaturization. The μDSS adopts a low-power windowing readout method: a two-step acquisition–tracking operation. The power consumed in the acquisition mode is significantly reduced with a profiling method which is enabled by a specific pixel design. The high accuracy is achieved by reducing the system thermal noise with a quadruple sampling method. The radiation hardness is strengthened by both hardware design and algorithm correction. The system miniaturization is realized by a SoC solution: integrating the active pixel sensor, timing control circuit, algorithm and processing circuit, and analog-to-digital converter on chip. The proposed μDSS achieves a 0.01° accuracy with 21 mW at 10 frame/s.**

***Index Terms*—CMOS image sensor, digital sun sensor, profiling.**

I. Introduction

FOR A spacecraft, its attitude information needs to be monitored during operation. Sun sensors are a specific category of attitude sensors that detect the orientation of the spacecraft by sensing the angular position with respect to the sun. A digital sun sensor can be constructed with a pinhole camera, as shown in Fig. 1 [1]–[3]. Sunlight illuminates a pixel array through a pinhole. Different pixels on the array are illuminated depending on the sunlight incident angle. The orientation information can be derived from the projective image on the detector's plane.

The system sketch in Fig. 1 illustrates the relation between the centroid of the projected sunspot and the sunlight incident angle. Here, l is the distance between the sunspot centroid and the center of the pixel array; F is the focal length, which is 1085 μm in the microdigital sun sensor (μDSS); and θ is the sunlight incident angle. The relation between l, θ, and F is

$$l = \tan(\theta) \bullet F \Rightarrow \theta = \arctan\left(\frac{l}{F}\right). \quad (1)$$

Since F is a constant value, θ can be expressed as a function of l. Thus, after l is determined by centroid detection, the respective angle between the satellite and the sun can be calculated by the processing circuits.

Manuscript received May 13, 2012; revised July 22, 2012; accepted August 27, 2012. Date of publication October 9, 2012; date of current version November 16, 2012. The review of this paper was arranged by Editor J. R. Tower.

N. Xie is with the Delft University of Technology, 2600 AA Delft, The Netherlands.

A. J. P. Theuwissen is with the Harvest Imaging, 3960 Bree, Belgium and also with the Delft University of Technology, 2600 AA Delft, The Netherlands.

Color versions of one or more of the figures in this paper are available online at http://ieeexplore.ieee.org.

Digital Object Identifier 10.1109/TED.2012.2216530

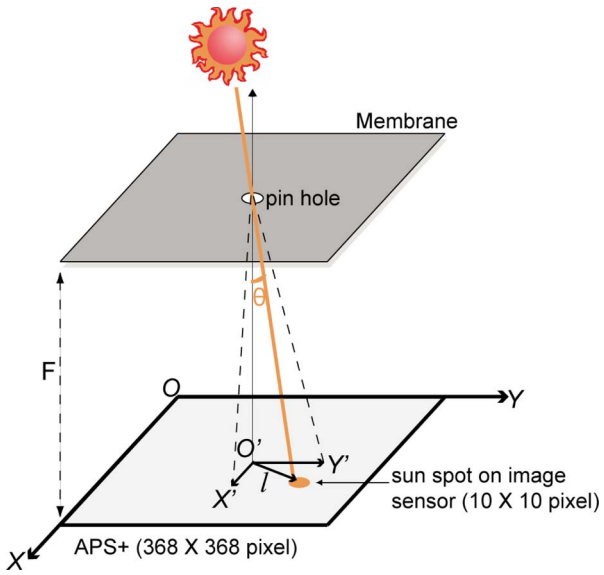

Fig. 1. System sketch of the μDSS.

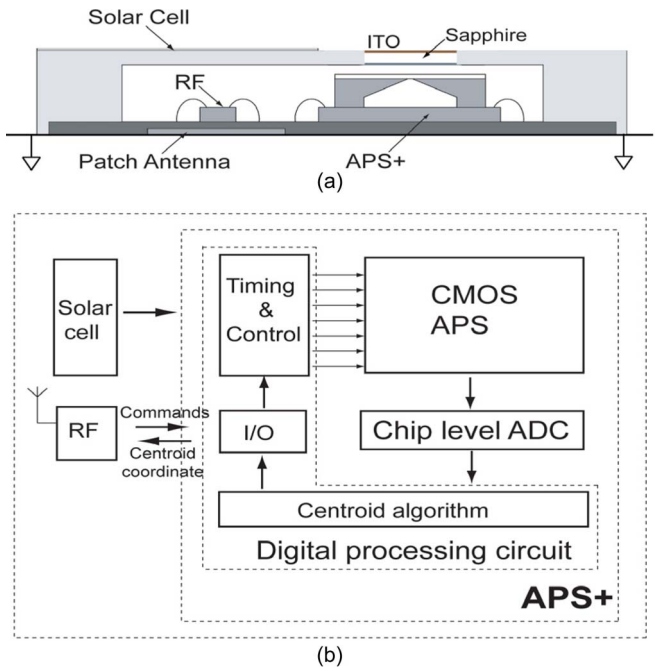

Fig. 2. (a) Cross section of the μDSS. (b) Block diagram of the μDSS.

A block diagram of the μDSS is presented in Fig. 2. The final goal of the μDSS is to have a fully autonomous and wireless sun sensor in one package, integrated with an imaging component, a solar cell unit, and an RF communication unit. The CMOS

0018-9383/$31.00 © 2012 IEEE

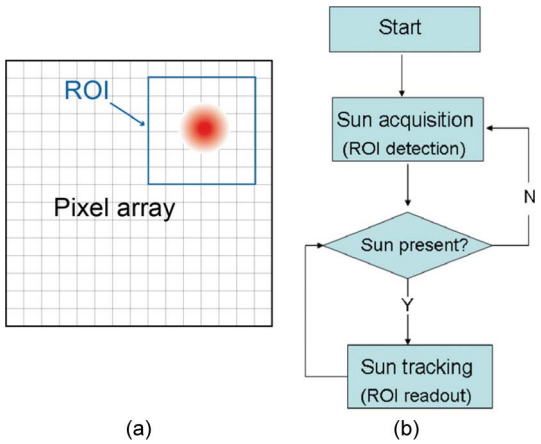

Fig. 3. (a) Illustration of pixel array and ROI. (b) Flowchart of the μDSS.

image sensor in the defined system, which is called APS+, is composed of three blocks: a CMOS active pixel sensor (APS), a chip-level ADC, and a digital circuit including the centroid algorithm and the timing and control circuits.

II. Overview of Working Principle

A. Overview of the Acquisition–Tracking Operation

As indicated in Fig. 1, the size of the illuminated sunspot is approximately 10 × 10 pixels while the complete pixel array is 368 × 368. In order to reduce power consumption, the μDSS has adopted a power-saving readout method: a two-step acquisition–tracking (coarse–fine) readout operation. First, in the acquisition mode, the coarse sun coordinates are estimated, and a region of interest (ROI) is determined. Afterward, in the sun tracking mode, the final centroid coordinates of the sunspot are determined based on the readout result of the ROI. An illustration of the ROI and the working flowchart are presented in Fig. 3.

B. Determining the FoV

The field of view (FoV) that is achieved by the μDSS is determined by the size of the pixel array. Equation (1) reveals the relation between the incident angle (θ) and the sunspot displacement (l). Since the tangent function is not linear, the displacement shift is larger when the sunlight incident angle becomes larger. This relation is shown in Fig. 4(a). The original FoV specification was ±56°. As is shown, in order to achieve a ±56° FoV, the range of the displacement l must be ±1.61 mm. Thus, with a pixel pitch of 6.5 μm, the minimum required pixel array size is 512 × 512. However, in practice, the limited chip area is not large enough for a 512 × 512 pixel array and its readout circuit. For this reason, in the prototype APS+ introduced in this paper, the real pixel array size is 368 × 368. With this pixel array, the available FoV becomes ±47°.

C. Determining the Size of the ROI

The ROI should be large enough so that sufficient sunlight-intensity information can be achieved for centroid calculation.

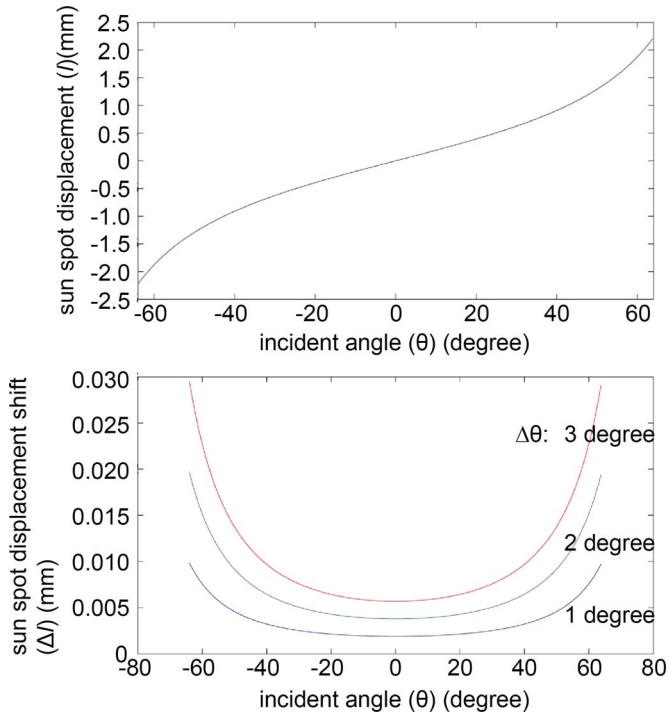

Fig. 4. (a) Relation between the sunspot displacement (l) and the incident angle (θ). (b) Relation between the displacement shift (Δl), the incident angle (θ), and the angular variance $(\Delta\theta)$.

In addition, as indicated in Fig. 3, since the ROI is decided in the acquisition mode but readout is decided in the tracking mode, the sunspot centroid could change during the mode-switching time. Therefore, the displacement shift due to the change in the satellite's position should also be considered when the ROI is decided. However, if the ROI is too large, the extra pixel noise as well as the readout noise are introduced into the calculation. Thus, a compromise has to be made when the ROI size is being determined.

The size of the sunspot is defined by the pinhole, which is approximately 10 × 10 pixels. The displacement shift (Δl) is decided by the incident angle (θ) and the angular variance during the time interval $(\Delta\theta)$. Their relation can derived from (1)

$$\Delta l = \frac{F}{\cos^2\theta} \bullet \Delta\theta = \frac{F}{\cos^2\theta} \bullet \frac{\partial\theta}{\partial t} \bullet \Delta t \tag{2}$$

where $\partial\theta/\partial t$ is the instant angular velocity of the satellite and Δt is the time interval. The relation in (2) is illustrated in Fig. 4(b). In this figure, the displacement shifts under three angular variances (1°–3°) are presented. The figure shows that this relation is also not linear. With the same angular variation, the displacement shift differs depending on the incident angle.

In the μDSS application, the satellite circles the Earth in a low Earth orbit in about 90 min. Thus, the normal angular velocity is $360/(90 * 60) = 0.07°/\text{s}$. However, in reality, the angular velocity is influenced by disturbances caused by variations in the Earth's magnetic field or the attitude changing operation of the satellite. In these situations, the large instant angular velocity $(\partial\theta/\partial t)$ could lead to significant angle variance $(\Delta\theta)$ in the short time interval between acquisition and

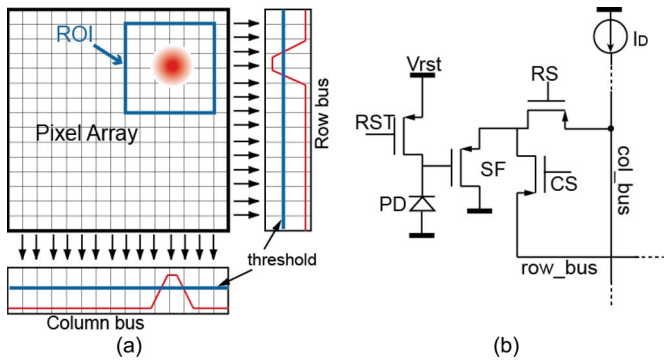

Fig. 5. (a) Profiling achieved by the μDSS; (b) pixel structure.

tracking modes. In a harsh environment, the angular variance could be up to 3°. In this case, considering the largest incident angle of $\pm 56°$ in Fig. 4(b), the displacement shift will be no more than ± 5 pixels (0.03 mm).

In conclusion, considering the sunspot size and the displacement shift in a harsh environment, a ROI with 21 $\times$ 21 pixels satisfies all the requirements. In practice, a window of 25 $\times$ 25 pixels will be read out, with two redundant pixels at each side of the ROI.

III. Low-Power Approach to the Acquisition Mode

The μDSS is specifically designed for microsatellite application, which has a rigid power consumption budget due to the limited size of the solar cell able to be carried on a microsatellite. Thus, low power is a major consideration in the μDSS design. The conventional readout method of formal digital sun sensors determines the sunspot centroid based on the readout result of the complete pixel array. The power consumption of such a digital sun sensor can be the order of several watts [4]. In recent years, some digital sun sensors have adopted an acquisition–tracking readout method similar to the μDSS [5]. However, during the acquisition operation, these digital sun sensors achieve the ROI by searching through the complete pixel array and comparing each pixel's amplitude with a predefined threshold level. This operation leads to a readout frequency much higher than the frame rate. Thus, the power consumed by the acquisition mode is normally twice that of the tracking mode [6].

In the μDSS, the power consumption in the acquisition mode needs to be further reduced. In some position-sensitive devices, the ROI is detected using an image projection technique [7]. In the APS+, the ROI is decided by a profiling method, which is achieved by the winner-take-all (WTA) principle, as shown in Fig. 5(a) [1]. The WTA is a computational principle which selects the largest input in magnitude from a set of inputs [8]–[10]. Many image sensors adopt an additional WTA circuit network to determine the ROI [11]. However, in the APS+, the WTA is achieved by the specific pixel architecture, as shown in Fig. 5(b), without an extra network circuit. The pixel in the APS+ is similar to a typical 3-T APS, but it has two major differences: First, the pixel is composed of only p-MOS transistors to execute the WTA principle, and second, in each pixel, an extra column select transistor is added besides the conventional row select transistor (RS) in order to enable row profiling.

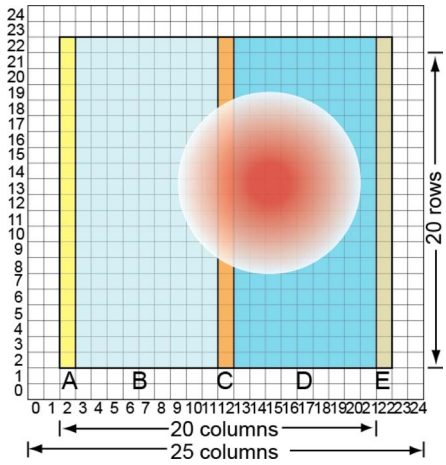

Fig. 6. Illustration of the centroid algorithm.

By this specific pixel design, the ROI can be achieved in an equivalent readout time of two lines; thus, the readout frequency is significantly reduced, leading to low power consumption [1], [3]. In the μDSS, the power consumed during acquisition is reduced to the same level as that in the tracking mode.

IV. Operation in the Tracking Mode

In the sun tracking mode, the CMOS APS reads out the ROI, and the algorithm circuit calculates and outputs the final centroid coordinates. The position resolution of the APS+ is a 1/64 pixel pitch.

A. Introduction to the Centroiding Algorithm

There are many centroiding algorithms that can determine the center point, for example, the threshold method, the image filtering method, and the template method [12], [13]. The algorithm needs to compromise between accuracy and hardware complexity. The centroiding algorithm implemented in the APS+ employs a "double balance" method, as shown in Fig. 6 [14]. The active ROI has 21 $\times$ 21 pixels, while the complete window has 25 $\times$ 25 pixels. The ROI is divided into several areas; they are labeled from A to E in the figure and are designated by different colors.

It is assumed that

$$S_{\mathrm{XA}} = \text{sum of pixel output in area-A } (1 \times 21 \text{ pixels})$$

$$S_{\mathrm{XB}} = \text{sum of pixel output in area-B } (9 \times 21 \text{ pixels})$$

$$S_{\mathrm{XC}} = \text{sum of pixel output in area-C } (1 \times 21 \text{ pixels})$$

$$S_{\mathrm{XD}} = \text{sum of pixel output in area-D } (9 \times 21 \text{ pixels})$$

$$S_{\mathrm{XE}} = \text{sum of pixel output in area-E } (1 \times 21 \text{ pixels}).$$

The centroiding is determined by two subwindows in the ROI. First, a window of 20 $\times$ 20 pixels is created around the pixel in the center of the ROI, which consists of areas A, B, C, and D. Next, the window is shifted by one column. This second

window consists of areas B, C, D, and E. Areas A and E are expected to be nonilluminated areas. As long as the background is uniformly distributed, it can be assumed that $S_{\mathrm{XA}} = S_{\mathrm{XE}}$. With this assumption, X_{POS}, which is defined as the centroid location referring to the center of the ROI, can be determined by the centroiding algorithm [14]

$$X_{\mathrm{POS}} = \frac{1}{2} \times \frac{S_{\mathrm{XD}} - S_{\mathrm{XB}}}{S_{\mathrm{XC}} - S_{\mathrm{XA}}}. \tag{3}$$

X_{POS} is expressed in pixel units. If the centroid is to the right of the ROI center, $X_{\mathrm{POS}} > 0$; if the centroid is to the left of the ROI center, $X_{\mathrm{POS}} < 0$. The centroid position referring to the ROI center on the y-axis, Y_{POS}, can also be determined in the same way as X_{POS}.

There are many noise sources in the APS+ image sensor. The algorithm resolution is determined by the thermal noise floor. The dark noise measurement discussed in Part B shows that the APS+ is able to achieve a resolution better than 1/64 pixel pitch, which is the design specification.

B. Low Noise Approach to the Tracking Mode

In order to improve noise performance, the APS+ implements the quadruple sampling (QS) method in the tracking mode, which reduces the reset noise and 1/f noise [3]. The measurement result shows that the thermal noise measured with QS is 24% better than that measured with the conventional delta double sampling (DDS) method. The thermal noise floor of the APS+ is 1650 μV with DDS and 1250 μV with QS. When saturated, the pixel output is 360 mV. Thus, the dynamic range achieved by the APS+ is 49.2 dB.

The X_{POS} deviation due to the measured noise floor of the QS can be derived from (3), which is ± 0.002 pixels. Under this condition, the APS+ thermal noise floor is not a limitation to the resolution specification of 1/64 pixels = 0.016 pixels. Instead, the photon shot noise becomes the dominant noise, which results in diminished accuracy compared to the resolution. The measurement result shows that the final accuracy achieved by the APS+ is 0.01° in the incident angle, which is referred as a 0.039 pixel pitch in placement (at room temperature).

V. Radiation Hardness in the μDSS

Although the power consumption is the major challenge for the μDSS design, radiation tolerance must also be carefully considered since the sun sensor will be implemented in space applications [15]. In the system design, the μDSS is shielded by an aluminum package that is a couple of millimeters thick, which is shown in Fig. 7(b). In addition, on top of the sapphire window, which is not shielded by the aluminum, an indium tin oxide (ITO) layer is deposited, as shown in Fig. 2(a). The ITO layer is a transparent conducting oxide layer which is connected to the grounded housing. With this layer, the sunlight can pass through the pinhole and reach the APS+ surface, while the charge generated by cosmic radiation is discharged through the housing.

With the system protection design, the radiation specification of the APS+ is reduced to the order of 20 to 30 krad, which will allow it to operate normally in a low Earth orbit for two to three years.

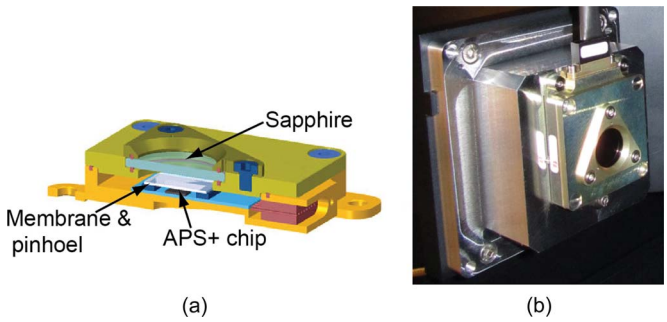

Fig. 7. (a) Cross section of the device and (b) picture of the APS+ packaged in housing.

The APS+ is manufactured with a TSMC 0.18-μm CMOS process. Some in-house radiation measurements have been done with image sensors produced by this process [16]. The results prove that this process intrinsically has a radiation tolerance up to 100 krad, which is higher than the required specification. Thus, in this application, the design challenges do not come from the total dose effect but come from single event upsets (SEUs) and potential single event latch-ups (SELs). Several hardware radiation-resistant designs and algorithm correction approaches have been implemented in the APS+ for SEU and SEL protection.

All in-pixel transistors are realized by a p-MOS, as shown in Fig. 5. Aside from the profiling method requirement [2], the p-MOS is also selected for radiation consideration. In the μDSS application, positive charges are trapped in the gate oxide due to cosmic radiation, leading to a net positive gate voltage; a p-MOS transistor remains off by the positive gate charges. By utilizing p-MOS transistors, the "dead" pixel introduced by radiation can be disconnected from the readout circuit, and thus, the influence of the "dead" pixel can be eliminated.

Meanwhile, in order to prevent a SEL, the pixel layout is sophisticatedly designed. A SEL is usually triggered by an unexpected current which is injected into the substrate through a junction capacitance, changing the substrate voltage. In the layout, two extra contacts in each pixel, which are connected to the n-well and p-substrate, are used to keep the well and substrate at the proper voltage levels. In this way, a potential latch-up is prevented.

If the SEU is not completely prevented by the hardware designs, the SEU-caused single pixel effect will be corrected by the APS+ algorithm. When a defect pixel occurs, it is detected by checking the intensity of the pixel with respect to the neighboring pixels. If the pixel intensity varies by more than 25% from the average of the neighboring pixels, the pixel will be "judged" as a defect pixel, and its value will be replaced by the average of the neighboring pixels [17], [18].

With all hardware and software precaution designs, the APS+ is able to achieve the radiation specification without the enclosed gate layout approach.

VI. Measurement Result

The APS+ chip has been manufactured and packaged in housing with a membrane and a pinhole, as shown in Fig. 7. The

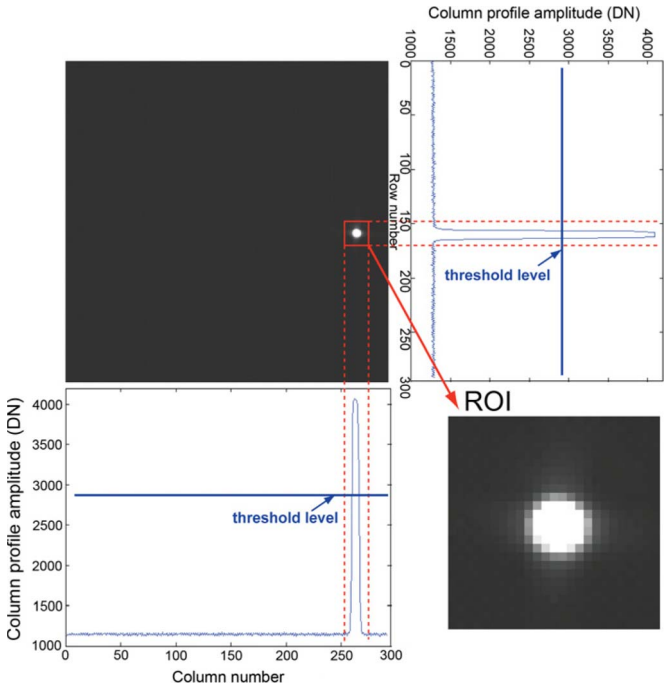

Fig. 8. Measurement result from the acquisition and tracking mode.

TABLE I
COMPARISON WITH THE STATE-OF-THE-ART

Characteristic	μDSS (This work)	Galileo (ESA) [6]
Year	2011	2009
Chip Size	5mm ×5mm	11mm ×11mm
Pixel Array	368 × 368	512 × 512
Integration	SoC	SoC
Power Consumption	21.34mW @ Acquisition 21.39mW @ Tracking	327mW @ Acquisition 193mW @ Tracking
Power Supply	3.3V for analog 1.8V for digital	3.3V for analog 1.8V for digital
FOV	±47°	±64°
Operating Temperature	-40°C to +80°C	-40°C to +70°C
Accuracy	0.01° (3σ)	0.024° (3σ)
Resolution	0.004°	<0.005°
Detection Principle	Digital sun sensor	Digital sun sensor

solar cell and RF block in Fig. 2 have not yet been integrated; thus, the APS+ communicates with an external PC through an RS-232 interface. A solar simulator (not presented in the picture) is used as the light source in the tests. The measurement result shows that the APS+ achieves a sun position accuracy of 0.01° (3σ). The profiling achieved in the acquisition mode and the ROI readout in the tracking mode are presented in Fig. 8.

The Galileo sun sensor in Table I is a digital sun sensor that also implements the pinhole detection principle [6]. Unlike the μDSS, this sun sensor addresses radiation hardness instead of power consumption. Thus, the enclosed gate layout is adopted and intrinsically leads to high power consumption. Its radiation specification reaches up to 2 M rad. However, power consumption has not been optimized in this design. Due to its scanning operation during the acquisition, the Galileo sun sensor consumes twice the power in the acquisition mode than in the tracking mode.

In comparison, low power is the highest priority in the APS+ design. The APS+ determines the ROI with the profiling method in the acquisition mode. By this means, the power consumed in the acquisition is reduced to the same level as in the tracking mode. It is shown in Table I that the μDSS continually consumes 21 mW in both of its operation modes.

VII. CONCLUSION

In conclusion, the proposed μDSS is a digital sun sensor for microsatellite application. It implements an acquisition–tracking operation mode. The power consumed during acquisition is significantly reduced with a profiling method, and the accuracy performance is improved with a QS method. It achieves a power consumption of 21 mW at 10 frame/s and an accuracy of 0.01° (3σ) with a FoV of $\pm 47^\circ$. In addition, radiation hardness is strengthened by both hardware design and algorithm corrections.

REFERENCES

[1] N. Xie, A. J. P. Theuwissen, B. Büttgen, H. Hakkesteegt, H. Jasen, and J. Leijtens, "Micro-digital sun sensor: An imaging sensor for space applications," in *Proc. IEEE ISIE*, 2010, pp. 3362–3365.
[2] N. Xie, A. J. P. Theuwissen, X. Wang, J. Leijtens, H. Hakkesteegt, and H. Jansen, "A CMOS image sensor with row and column profiling means," in *Proc. IEEE Sens. Conf.*, Oct. 2008, pp. 1356–1359.
[3] N. Xie and A. Theuwissen, "An autonomous low power high resolution micro-digital sun sensor," in *Proc. Int. Symp. Photoelect. Detection Imag.*, Beijing, China, May 24–26, 2011.
[4] T. Ding, Y. Bi, and P. Wang, "Micro-digital sun sensor with CMOS APS," *J. Tsinghua Univ. (Sci. Technol.)*, pp. 203–206, Feb. 2008.
[5] F. Boldrini, E. Monnini, and D. Rocopio, "Applications of APS detector to GNC sensors," in *Proc. 4th IAA Symp. Small Satellites Earth Observ.*, Berlin, Germany, Apr. 2003, pp. 33–40.
[6] F. Boldrini, E. Monnini, D. Procopio, B. Alison, W. Ogiers, M. Innocent, A. Pritchard, and S. Airey, "Attitude sensors on a chip: Feasibility study and breadboarding activities," in *Proc. 32nd Annu. AAS Guid. Control Conf.*, Breckenridge, CO, Feb. 2009, pp. 1197–1216.
[7] E. Funatsu, S. Kuramochi, Y. Nagafuchi, H. Kage, N. Sakashita, F. Murao, and K. Kyuma, "Artificial retina large scale integration with on-sensor projection function for high-speed motion detection," *Opt. Eng.*, vol. 41, no. 11, pp. 2709–2718, Nov. 2002.
[8] G. A. Carpenter and S. Grossberg, "A massively parallel architecture for a self-organizing neural pattern recognition machine," *Comput. Vis., Graph. Image Process.*, vol. 37, no. 1, pp. 54–115, Jan. 1987.
[9] V. Brajovic and T. Kanade, "Computational sensor for visual tracking with attention," *IEEE J. Solid-State Circuits*, vol. 33, no. 8, pp. 1199–1207, Aug. 1998.
[10] A. Mäkynen, T. Ruotsalainen, T. Rahkonen, and J. Kostamovaara, "CMOS-compatible position-sensitive devices (PSDs) based on photodetector arrays," *Sens. Actuators A, Phys.*, vol. 105, no. 3, pp. 261–270, Aug. 2003.
[11] A. Fish, D. Turchin, and O. Yadid-Pecht, "An APS with 2-D winner-take-all selection employing adaptive spatial filtering and false alarm reduction," *IEEE Trans. Electron Devices*, vol. 50, no. 1, pp. 159–165, Jan. 2003.
[12] C. Liebe and S. Mobasser, "MEMS based sun sensor," in *Proc. IEEE Aerosp. Conf.*, 2001, pp. 1565–1572.
[13] Y. Chang and B. Lee, "Development of high accuracy image centroiding algorithm for CMOS-based digital sun sensors," *Sens. Actuators A, Phys.*, vol. 144, no. 1, pp. 29–37, May 2008.
[14] C. de Boom, "Internal information by TNO," TNO, Delft, The Netherlands, May 2011.
[15] J. Leijtens, N. Xie, and A. Theuwissen, "The APS+ and why we dare going without DARE," in *Proc. 3rd Int. Workshop Analog Mixed Signal Integr. Circuits Space Appl.*, Noordwijk, Netherlands, Sep. 5–7, 2010.

[16] J. Tan, B. Büttgen, and A. J. P. Theuwissen, "Radiation effects on CMOS image sensors due to X-rays," in *Proc. Int. Conf. Adv. Semicond. Devices Mircrosyst.*, Smolenice, Slovakia, Oct. 2010, pp. 279–282.
[17] C. de Boom, J. A. P. Leijtens, L. M. H. v. Duivenbode, and N. van der Heiden, "Micro digital sun sensor: System in a package," in *Proc. Int. Conf. MEMS, NANO Smart Syst.*, Aug. 2004, pp. 322–328.
[18] J. Leijtens, K. de Boom, and N. van der Heiden, "Micro systems technology: The way to shrink sun sensors," in *Proc. Int. Conf. MEMS, NANO Smart Syst.*, Jul. 2005, pp. 193–194.

Ning Xie (S'10–M'12) received the B.S. degree in electrical engineering from Zhejiang University, Hangzhou, China, in 2004 and the M.Sc. and Ph.D. degrees from TU Delft, Delft, The Netherlands, in 2007 and 2012, respectively.

Albert J. P. Theuwissen (S'83–M'83–SM'95–F'03) received the Ph.D. degree in electrical engineering from the Catholic University of Leuven, Leuven, Belgium, in 1983.

In March 2001, he was appointed as part-time professor at the Delft University of Technology, Delft, The Netherlands.